applied sciences

MDPI

Article

An Image Denoising Technique Using Wavelet-Anisotropic Gaussian Filter-Based Denoising Convolutional Neural Network for CT Images

Teresa Kwamboka Abuya [1,*], Richard Maina Rimiru [2] and George Onyango Okeyo [2]

[1] Department of Computer Science, Jomo Kenyatta University of Agriculture & Technology, Nairobi P.O. Box 62000-00200, Kenya
[2] College of Engineering, Carnegie Mellon University, Kigali BP 6150, Rwanda; rimirurm@gmail.com (R.M.R.); george.okeyo@gmail.com (G.O.O.)
* Correspondence: tkwambokaa@gmail.com

Abstract: Denoising computed tomography (CT) medical images is crucial in preserving information and restoring images contaminated with noise. Standard filters have extensively been used for noise removal and fine details' preservation. During the transmission of medical images, noise degrades the visibility of anatomical structures and subtle abnormalities, making it difficult for radiologists to accurately diagnose and interpret medical conditions. In recent studies, an optimum denoising filter using the wavelet threshold and deep-CNN was used to eliminate Gaussian noise in CT images using the image quality index (IQI) and peak signal-to-noise ratio (PSNR). Although the results were better than those with traditional techniques, the performance resulted in a loss of clarity and fine details' preservation that rendered the CT images unsuitable. To address these challenges, this paper focuses on eliminating noise in CT scan images corrupted with additive Gaussian blur noise (AGBN) using an ensemble approach that integrates anisotropic Gaussian filter (AGF) and wavelet transform with a deep learning denoising convolutional neural network (DnCNN). First, the noisy image is denoised by AGF and Haar wavelet transform as preprocessing operations to eliminate AGBN. The DnCNN is then combined with AGF and wavelet for post-processing operation to eliminate the rest of the noises. Specifically, we used AGF due to its adaptability to edge orientation and directional information, which prevents blurring along edges for non-uniform noise distribution. Denoised images are evaluated using PSNR, mean squared error (MSE), and the structural similarity index measure (SSIM). Results revealed that the average PSNR value of the proposed ensemble approach is 28.28, and the average computational time is 0.01666 s. The implication is that the MSE between the original and reconstructed images is very low, implying that the image is restored correctly. Since the SSIM values are between 0 and 1.0, 1.0 perfectly matches the reconstructed image with the original image. In addition, the SSIM values at 1.0 or near 1.0 implicitly reveal a remarkable structural similarity between the denoised CT image and the original image. Compared to other techniques, the proposed ensemble approach has demonstrated exceptional performance in maintaining the quality of the image and fine details' preservation.

Keywords: denoising CNN; image denoising; additive Gaussian blur noise; CT images; wavelet transform; anisotropic Gaussian filter

Citation: Abuya, T.K.; Rimiru, R.M.; Okeyo, G.O. An Image Denoising Technique Using Wavelet-Anisotropic Gaussian Filter-Based Denoising Convolutional Neural Network for CT Images. *Appl. Sci.* **2023**, *13*, 12069. https://doi.org/10.3390/app132112069

Academic Editors: Xi-Le Zhao and Junmin Liu

Received: 27 August 2023
Revised: 24 October 2023
Accepted: 25 October 2023
Published: 6 November 2023

1. Introduction

Computed tomography (CT) is a widely used medical imaging modality that precisely identifies anatomical structures and abnormalities [1]. Medical imaging has revolutionized the healthcare sector by assisting medical professionals in several ways, such as in disease diagnosis, treatment, and risk prediction [2]. However, popular medical imaging modalities, such as magnetic resonance imaging (MRI), ultrasound (US) images, positron emission tomography (PET), and computed tomography (CT) images [2], are degraded by various

kinds of noise, not limited to Gaussian noise, speckle noise, Poisson noise, and salt and pepper noise, which severely affects fine details of an image, such as edges, lines, and points [3,4]. For instance, positron emission tomography (PET) is a procedure that involves nuclear imaging to provide information about the operation of different tissues and organs. These images are usually degraded by a low signal-to-noise ratio and blurred edges caused by Poisson and Gaussian noise. Similarly, CT medical images are corrupted by Gaussian and salt and pepper noise, among others. Gaussian blur noise in CT imaging is caused by electronic noise, image post-processing, the reconstruction process, and quantization [5].

Ultrasound is a medical imaging modality that uses high-frequency sound waves to create real-time images of the inside of the body. It is a non-invasive and safe imaging technique widely used for diagnostic and monitoring purposes. When ultrasound waves propagate through a biological medium, the images are contaminated with speckle noise, obfuscating the pertinent details and reducing the contrast of the soft tissues, thereby degrading their overall visual quality [6]. Medical image analysis encompasses various image types characterized by their generation and appearance, and each is affected by distinct noise that deteriorates their image quality.

The major challenge in the process of medical imaging is to obtain an image without loss of any meaningful information for decision-making. Noise or artifacts corrupt the images obtained during the acquisition and further processing stages [7]. Unlike natural images, most medical images pose signal-dependent noises; hence, it is hard to remove them by using conventional raw image denoising techniques [8]. Noise refers to the random variations of brightness and color that are not part of the original image, which deteriorates the image quality and even makes them diagnostically unusable [9]. The blurry and corrupt image quality reduces the visibility of structural details and discourages further decision-making, leading to poor diagnosis, analysis, and treatment [10].

Gaussian noise is the type of noise that arises from sensor noise, heat propagation, or circuit noise that affects CT scan images. Gaussian noise introduces random fluctuations in pixel intensity levels across the image, leading to a loss of image clarity, sharpness, and fine details' preservation and restoration [11].

When CT scan images are acquired, factors such as photon statistics, electronic noise, and patient motion can introduce noise into the images [12]. The noise can obscure fine details and reduce the overall image quality, leading to information loss [13]. The main aim of image denoising is to remove the noise while preserving the details of the image and cover aspects such as edge preservation and robustness to any artifacts [14]. In addition, denoising and enhancement of medical images can be helpful in image restoration, feature extraction, and in reducing distortion of images obtained from complex imaging modalities such as MRI, PET, and CT [15,16]. Several noise reduction approaches have been reported to address this problem during preprocessing and post-processing stages. These approaches include Gaussian filters (GF), mean filters (mean-F), median filters (Median-F), bilateral filters (BF), wiener filters (WF), non-local mean filters (NLM), and denoising convolutional neural networks (DnCNN) [17–20]. However, these conventional spatial filtering techniques [17–21] for image denoising are still faced with the challenge of preservation of image details, which causes the blurring effect, handling of complex noise patterns, parameter tuning, artifacts, and computational complexity, which affect their direct use for medical diagnostic purposes [20,21]. For instance, Vimala [22] proposed a dual-tree DWT combined with wiener filters, used for an image affected by white Gaussian noise, proving that DT-DWT and wiener filters effectively denoise white Gaussian noise. However, the estimation of sub-optimal characteristics led to sub-optimal denoising results. Zhang et al. [23] proposed a non-local (NL) means filtering scheme for Gaussian noise removal, where the resemblance of local patches determines the pixel weights. When the window size of the image is reduced to only a one-pixel value, the NL-means filtering becomes the same as the bilateral filter [24].

In [25,26], median filter and wavelet transform were applied to denoise CT scan images, and better results were achieved. However, there were challenges of blurring and detail

preservation, high computational complexity, and edge smudging, which affect the accurate diagnosis and distortion of critical anatomical structures. The DWT effectively reduces noise while preserving image details. However, as the authors of [27] pointed out, selecting an appropriate wavelet basis and thresholding strategy is crucial for balancing noise removal and detail preservation. In [28], mean filters (Mean-F) were used for denoising CT images. However, they blurred the edges and fine details of the image while reducing noise [29]. In [30], Gaussian filters effectively removed random additive noise, such as Gaussian noise, which follows a uniform Gaussian distribution [31]. They did not perform well for large CT scan images, which suffer from unwanted smoothing artifacts that lead to loss of fine details in the image, high computation costs, and blurring of the edges.

It is demonstrated that the significant challenges faced by filters in [17–31] were edge preservation, image restoration, computational intensity, and the blurring effect problem, which decreases image sharpness, obstructs the view of the underlying anatomy, and renders the CT scan images unsuitable. In recent years, several convolutional neural network (CNN)-based methods have been proposed for natural image denoising, and the application of a three-layer CNN for low-dose CT has shown promising results. Using a deep-CNN improves the image processing performance because of its strong symbolic power. However, when trained with a widely used pixel-level loss function, the CNN-based models often suffer from vanishing gradients by introducing blurring in denoising images [32]. Additionally, striking a balance between noise reduction and retention of clinically relevant information remains a challenge. Therefore, a wavelet-based image deblurring and restoration ensemble approach is proposed to enhance image quality, preserve edge information, and improve image restoration while eliminating the entire image noise.

The proposed ensemble approach uses the denoising capabilities of an anisotropic Gaussian filter (AGF), wavelet transform, and denoising convolutional neural network (DnCNN). The AGF is used as a preprocessing operation to reduce Gaussian noise in the image by selectively smoothing the image while preserving the edges and fine details, effectively reducing noise levels. When applied with suitable parameters, it helps reduce blurring effects in the image and restore sharpness. The Haar transform wavelet is a preprocessing operation known for preserving edges due to its ability to capture sharp transitions in the image. An inverse Haar transform is performed to reconstruct the enhanced image. The denoising CNN is trained on pairs of degraded images (blurred and noisy) and their corresponding clean, sharp versions. The CNN learns to map the degraded images to their clean counterparts, effectively removing the blurring effect and restoring the image. Both AGF and Haar transform inherently contribute to edge preservation, considering that the AGF preserves edges while selectively smoothing other regions, and the Haar transform allows for directional analysis, which can further enhance the edge preservation during the restoration process with the DnCNN. Anisotropic Gaussian filters adaptively adjust their parameters based on local image features, allowing for effective noise reduction without sacrificing important image details.

Main Contribution

This study strives to improve the results obtained in [24,32] by embodying the concept of the anisotropic Gaussian filter (AGF) and Haar transform as preprocessing operations. The studies in [24,32] presented a wavelet-Gaussian filter and a deep-CNN-based model to eliminate Gaussian and speckle noise. This study adopts an augmented methodology by implementing an anisotropic Gaussian filter, Haar wavelet transform, and DnCNN. The study contributes to the following aspects:

1. An ensemble approach is proposed using DnCNN, the anisotropic Gaussian filter (AGF), and Haar wavelet transform. The AGF and Haar transform are applied as preprocessing operations. The choice of AGF was primarily due to its adaptability to edge orientation, adaptive filtering, and directional information, effectively handling

edges based on gradient magnitude and preventing blurring along edges commonly encountered with standard filters.
2. The ensemble approach demonstrates better results when compared to CNN-based methods and other standard spatial filtering techniques in reducing the blurring effect and improving image quality and restoration.

2. Related Work

Noise in medical images refers to unwanted random variations or distortions superimposed on the underlying image information. It degrades the quality and clarity of images, making it challenging to accurately interpret and analyze them [33]. Noise can arise from various medical imaging sources, including imaging equipment, signal acquisition, patient factors, and image processing [34]. Image denoising aims to obtain the best of an original image from the corrupted image. Noise reduction improves the perception of images and usually results in better performance for different image analysis and computer vision algorithms [35]. In [36], the authors pointed out that during the transmission of medical images, noise becomes a dominant factor that deteriorates and degrades the image's contrast, reducing its quality and appearance and creating problems in the diagnostic phase. Salt and pepper noise (SPN) and Gaussian noise (GN) are common types of noise in medical images that occur in acquisition or data transmission through any network or medium [37–39]. Usui et al. [40], in their quantitative evaluation of deep convolutional neural network-based image denoising for low-dose computed tomography, eliminated Gaussian noise, and maintained sharpness using DnCNN.

In [41], Gaussian noise was added with a standard deviation of 0.002 to thoracic CT images. A fast, non-local means (FNLM) denoising algorithm removed blurring in the images. The FNLM was more efficient than conventional denoising filters, such as Gaussian, wiener, and median filters. Sarita et al. [42] assessed denoising filters for brain MRI-weighted contrast-enhanced images. The PSNR, SSIM, and MSE are statistical parameters used for analyzing the performance of the filters. The study showed that the wiener filter is considered the most efficient for Gaussian noise. In the case of speckle noise, anisotropic filters work better on low noise density, whereas the Gaussian filter works better for high noise density. Wang et al. [43] used adaptive wavelet transform and CNN for image denoising, and PSNR was calculated as high and MSE as low. In addressing Gaussian and Rician noise issues of data loss due to compression and preservation of edge details, Juneja et al. [44] used Bayesian shrinkage-based fused wavelet transform (BSbFWT) and the block-based autoencoder network (BBAuto-Net) to remove noise from MRI. A novel algorithm that combines the bilateral filter and its method of noise thresholding, using dual-tree complex wavelet transform to remove Gaussian noise in the image, was proposed by Majeetah et al. [45]. The experimental results show that the proposed algorithm is superior to other existing filtering algorithms in terms of visual quality and has very good PSNR, SSIM, and UIQI values. However, the issues around image blurring, contrast reduction, and quantitative inaccuracies of PSNR and SSIM were not adequately addressed.

The CNN and bilateral filters were used to remove Gaussian noise from CT images in [46], and the authors of [47] presented a novel window-based method to remove high-density salt and pepper noise for optimal ROI (region of interest) detection of the brain MRI images. The output was used in watermarking and extracting hidden data in this type of image. An impulse noise removal algorithm model was proposed based on logarithmic images before medical images [48]. Experimental results using PSNR and MSE showed that the method was superior in terms of the effectiveness of impulse noise (salt and pepper noise) removal for medical images, CT, or MRI [49]. In [50], they developed a fast method based on Fuzzy Logic for Gaussian impulsive noise reduction in CT medical images. By applying parallel computing strategies, the obtained computing times indicated that the introduced filter reduced Gaussian–impulse-mixed noise on CT medical images in real time. In [51], the authors discussed how Gaussian filters effectively removed random additive noise, such as Gaussian noise that follows a uniform Gaussian distribution. However, they

did not perform well in the presence of other types of noise, such as impulse noise, which caused blurring around edges and introduced halo-like artifacts in the denoised image [52]. The blurring and halo artifacts can distort the fine details of objects and degrade the overall visual quality of the image.

Gaussian noise often distorts digital images, which is an essential problem in image processing. In [53], the impulse and Gaussian noise in the CT image were removed based on the edge-preserving median filter algorithm. The sparse, non-local regularization algorithm weighted coding was used to remove the impulse and Gaussian noise in the mixed noise, and the peak signal-to-noise ratio (PSNR) and structural similarity index (SSIM) were calculated to evaluate the quality of the denoised CT image. The performance of the median filter for Gaussian noise removal could have been more effective due to its discrete nature, acceptable detail loss, and edge preservation. Authors in [23–27,41–53] discussed the challenges of image denoising based on the state-of-the-art medical image denoising techniques, such as bioinspired optimization-based filters and spatial filters using CNN, which included the preservation of image details, trade-off between noise removal and detail preservation, noise characteristics, computational complexity, and spatial and temporal coherence. However, these conventional image denoising techniques do not remove additive Gaussian noise from CT scan images because these spatial filters and denoising techniques [23–27,41–53] may excel at reducing noise but need help to maintain the integrity of intricate anatomical information.

Conversely, filters that prioritize preserving details might not adequately reduce noise, making images challenging to interpret. To this end, we propose an ensemble approach that uses DnCNN, anisotropic Gaussian filters, and Haar wavelet transform. By leveraging the strengths of each technique, the proposed ensemble approach achieves superior denoising performance, preserving image details while effectively suppressing the noise.

3. Methodology

CT images often suffer from Gaussian blur noise and streak artifacts that reduce image quality, affect image analysis, obfuscate image information, and compromise diagnostic confidence. With that assumption, a wavelet–AGF-based image deblurring and restoration ensemble approach is proposed. Here, a denoising DnCNN that leverages deep learning architectures and image processing techniques that reduce the blurring effect and edge preservation is tailored for this study [54]. This framework is trained to denoise images corrupted with additive Gaussian blur noise (AGBN). Unlike the conventional denoising models, the combination of the anisotropic Gaussian filter (AGF) and Haar wavelet transform allows different standard deviations along different directions, making it capable of preserving edges while simultaneously reducing blurring. The Haar wavelet transform is preferred over other transform methods because it effectively preserves edges and fine details in images. This is particularly advantageous when dealing with CT images, which often contain essential anatomical and structural edges that must be preserved during denoising.

Combining Haar wavelet, anisotropic Gaussian filters, and DnCNN leverages the strength of each component: Haar wavelet for preserving structural details, anisotropic Gaussian filters for noise reduction while maintaining edges, and DnCNN for capturing complex noise patterns. Here, both spatial and frequency domain information are addressed.

The additive Gaussian blur noise is evenly distributed through the imagery plane with various density values following the normal distribution “bell-shaped curve”. which has a shape reminiscent of a bell. Mathematically, the addition of Gaussian blur noise (GBN) can be shown as:

$$m(x,y) = i(x,y) + n(x,y) \quad (1)$$

where $i(x, y)$ is the original signal, $n(x, y)$ is the added noise, and $m(x, y)$ is the final image, with (x, y) determining the pixel location in the viewpoint plane. The bell-shaped curve

follows a probability density function (PDF) representing an image's statistical distribution of pixel intensities. It is represented as:

$$F(g) = \frac{1}{\sqrt{2\pi\sigma^2}} e^{-\frac{(g-\mu)^2}{2\sigma^2}} \tag{2}$$

where g = gray level, $F(g)$ represents the probability density function, μ = mean, and σ = standard deviation of the noise. The noisy CT image "image1.jpg" is loaded, and the noise level (σ) is extracted from the image, where σ = 0.15. The anisotropic Gaussian filter is used to suppress Gaussian blur noise from the input image to enhance the quality of the CT scan medical images. The mathematical formula for the anisotropic Gaussian filter is given by:

$$G(x, y) = \exp\left(-\frac{x^2 + y^2}{2 * \sigma^2}\right) \tag{3}$$

where $G(x, y)$ is the Gaussian filter kernel, (x, y) are the spatial coordinates, and σ is the noise standard deviation from the noisy image.

Here, the AGF is applied as a preprocessing step to reduce AGBN in the image by adaptively adjusting the filter parameters based on local image features.

Noise standard deviation: σ = 0.15 (extracted from the noisy image)

Anisotropic Gaussian filter kernel: $G(x, y) = \exp(-2\sigma^2 \times 2 + y^2)$

$$G(xy) = \exp\left(-\frac{x^2 + y^2}{2\sigma^2}\right) \tag{4}$$

These parameters describe the noise standard deviation (2σ) and the mathematical formula for the anisotropic Gaussian filter kernel ($G(x, y)$). The filter kernel suppresses Gaussian blur noise in the input image to enhance the quality of the CT scan medical images.

After noise reduction with the AGF, the Haar transform is used as a preprocessing step for further noise reduction by performing a 2D discrete wavelet transform (DWT) on the denoised image using the Haar wavelet transform. The 2D DWT Haar wavelet transform decomposes the image into approximation (LL) and detail (LH, HL, HH) sub-bands. The DWT coefficients are computed using the Haar wavelet, and the formula for DWT is given by:

$$C(i, j) = \frac{1}{2} * (A(i, 2j) + A(i, 2j + 1)), \text{ for the LL sub-band}$$

$$C(i, j) = \frac{1}{2} * (A(i, 2j + 1) - A(i, 2j)), \text{ for the LH sub-band}$$

$$C(i, j) = \frac{1}{2} * (A(2i, j) - A(2i + 1, j)), \text{ for the HL sub-band}$$

$$C(i, j) = \frac{1}{2} * (A(2i, 2j) + A(2i + 1, 2j) - A(2i, 2j + 1) - A(2i + 1, 2j + 1)), \text{ for the HH sub-band} \tag{5}$$

where $A(i, j)$ are the pixels of the denoised image and $C(i, j)$ are the DWT coefficients. In inverse discrete wavelet transform (IDWT), the 2D IDWT is applied to combine the denoised detail sub-bands with the original approximation sub-band to reconstruct the final denoised CT scan images. Setting coefficients below a specific threshold value to zero helps remove noise by identifying regions affected by blurring while retaining image details. Image deblurring was applied on Haar transform coefficients for restoring lost high-frequency details, effectively reducing the blurring effect. The architecture of the proposed approach is shown in Figure 1.

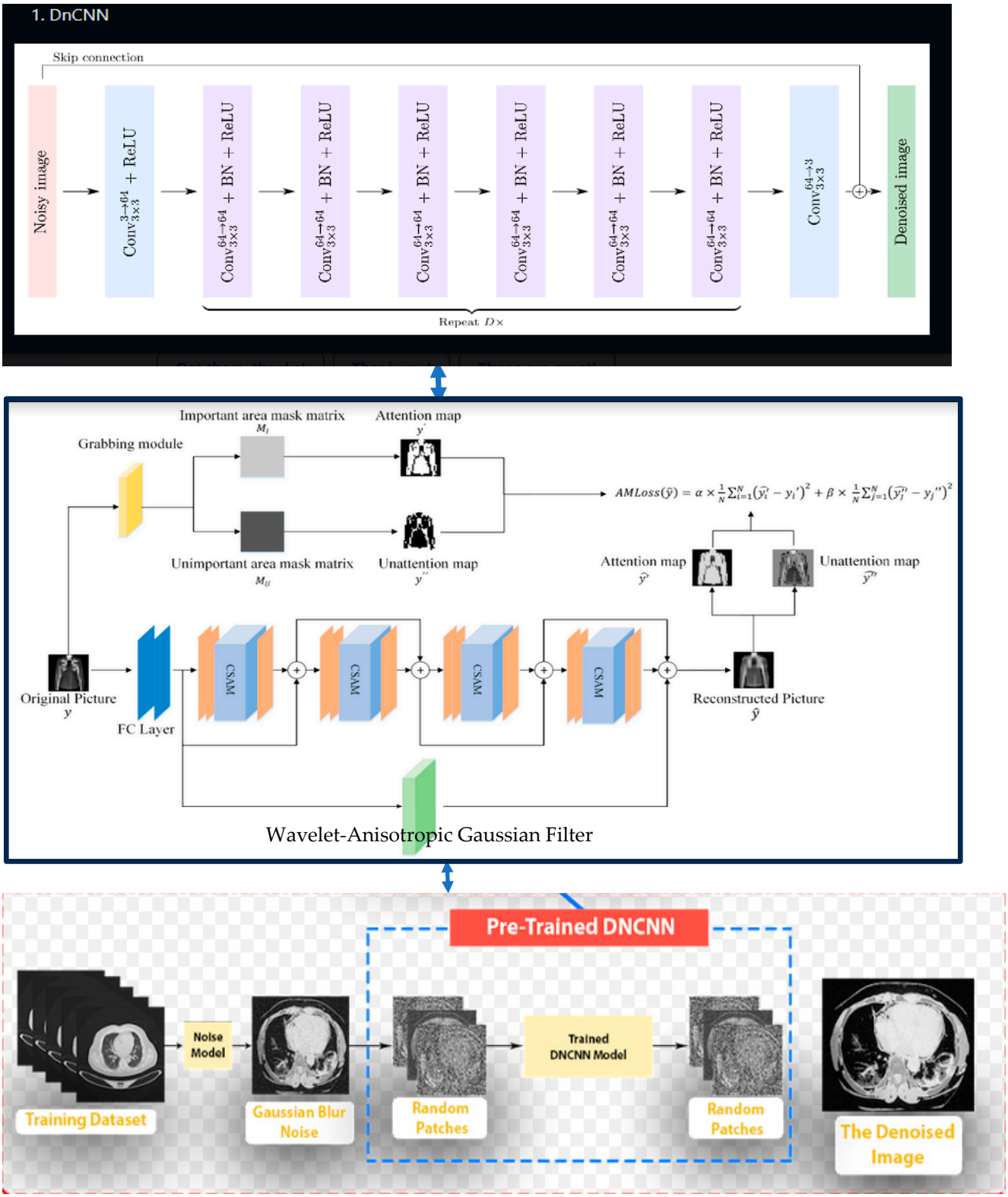

Figure 1. The architecture of the proposed ensemble denoising approach.

Step 1 (input original image): read authentic CT scan images.
Step 2 (perform initial noise detection): Use the anisotropic Gaussian filter (AGF) to gauge the level of Gaussian noise in the initial test when checking for the type of noise in the images. It smoothens images while preserving the edges and details, effectively reducing noise levels.

Step 3 (add Gaussian blur noise): read noisy corrupted CT scan images.
Step 4 (perform DnCNN): the general CNN process is given below:

a. Design a denoising CNN with skip connections to preserve low-level image details during denoising.
b. Implement batch normalization and ReLU activation after each convolutional layer to improve training stability.
c. Use residual blocks to capture and learn essential image features.
d. Implement skip connections to pass relevant information across different layers.

The CNN architecture uses convolutional layers with batch normalization and ReLU activation functions. The skip connections are implemented using residual blocks. The output of each residual block is obtained as follows:

$$R(x) = F(x) + x \tag{6}$$

where $R(x)$ is the residual block output, $F(x)$ is the output of the convolutional layers, and x is the input to the residual block.

Gradient-based algorithms, such as stochastic gradient descent (SGD), optimize the DnCNN model in finding the best values for the filters used to train the weights. The following loss function is used to minimize the error:

$$l(\theta) = \frac{1}{2N} \sum_{i=1}^{N} \| R(y_i;\theta) - (y_i - x_i) \|_F^2 \tag{7}$$

The DnCNN architecture above has three layers, each corresponding to a different function.

Layer 1: Convolutional layers with ReLU, 64 filters each of dimensions $3 \times 3 \times$ (No. of channels), weaving their intricate patterns to produce 64 feature maps, each imbued with the essence of rectified linear units. The gray image summons one channel, while the color image demands three (RGB) channels.

Layer 2: Convolutional layers, with ReLU batch normalization (BN), added between each convolutional and ReLU layer. The 64 additional filters intertwine, taking the form of $3 \times 3 \times 64$ dimensions.

Layer 3: The final convolutional layer stands as the key to unlocking the realm of image reconstruction. The 64 elusive filters, each with a size of $3 \times 3 \times 64$, collaborate to peer into the depths and bring forth reimagined images.

Step 5 (perform denoising):

a. Apply the designed CNN to each detail sub-band obtained from the wavelet decomposition (LH, HL, HH).
b. Set the denoising threshold for each sub-band based on the noise level (σ) obtained in the preprocessing step. For example, set the point as 0.1. The threshold value is a determinant of the image used for the experiments, and in this study, a value of 0.05 was used. The value was chosen to demonstrate the concept of thresholding and its impact on image denoising. Factors such as noise characteristics and specific image content should be empirically determined in an experiment.
c. Perform soft thresholding on the CNN output for each sub-band to reduce noise and preserve critical features.
d. Denoising uses soft thresholding on the CNN output for each detail sub-band. The soft thresholding formula for denoising a sub-band is given by:
e. C_denoised (i, j) = sign $(C(i, j)) * \max(|C(i, j)| - \lambda, 0)$
f. Where C_denoised (i, j) are the denoised DWT coefficients, $C(i, j)$ are the original DWT coefficients, and λ is the wavelet threshold.

The relationship between the denoising threshold and the noise level (σ) for each sub-band in the denoising process can be summarized as follows:

i. Denoising threshold: the denoising threshold (λ) is a parameter that determines the level at which noisy coefficients in each sub-band will be attenuated or suppressed during the denoising process.
ii. Noise level (σ): The noise level (σ) represents the standard deviation of the noise present in the image. It characterizes the amount of noise contamination in the image, such as Gaussian blur noise.
iii. Relationship: The denoising threshold (λ) is typically set based on each sub-band's estimated noise level (σ). The choice of the denoising threshold is critical because it determines which coefficients are considered noise and should be reduced or eliminated.
    - If λ is set too high, it may remove essential image details, leading to over-smoothing and loss of image information.
    - If λ is too low, it may not effectively suppress the noise, resulting in noisy artifacts in the denoised image.

Therefore, to strike a balance, the denoising threshold is often determined empirically or based on the statistical properties of the noise in each sub-band. It should be chosen to reduce noise while preserving essential image features and fine details. The relationship between the denoising threshold (λ) and the noise level (σ) is that λ is a parameter adjusted based on the estimated noise level in each sub-band to achieve effective noise reduction without excessive loss of image quality. The specific threshold value may vary depending on the noise characteristics and the desired level of denoising.

Step 6 (Haar wavelet transform)

A wavelet-based Haar transform is used for further noise reduction, where the additive noise is decomposed into one low-frequency sub-band image (LL2) and six high-frequency sub-band images (LH1, HL1, HH1 LH2, HL2, and HH2) while using a two-level Haar transform. In the wavelet domain, horizontal (HL1, HL2) and vertical (LH1, LH2) sub-band images have the same energy. Horizontal and vertical sub-band images were applied to soft thresholds to remove additive Gaussian blur noise. Removing noise and lower-frequency components while retaining high-frequency information related to the edge helps enhance edge details and reduce blurring. The soft thresholding in additive Gaussian blur noise is applied to suppress noise in an image by shrinking a small-magnitude coefficient, leaving more significant magnitude coefficients unchanged. A threshold value is applied and sets all coefficients below this threshold to zero, effectively reducing the noise level while preserving important signal information.

Step 7 (inverse wavelet transform):

a. Combine the denoised detail sub-bands with the original approximation sub-band.
b. Perform the 2D inverse discrete wavelet transform (IDWT) to reconstruct the final denoised CT image.
c. The 2D IDWT combines the denoised detail sub-bands with the original approximation sub-band to reconstruct the final denoised CT image.

Further, the DnCNN is combined with AGF and wavelet Haar transform for post-processing. The CNN uses convolutional layers that slide across the image, analyzing small local patches simultaneously, allowing the network to capture local context and spatial information for preservation. Since DnCNN learns to represent images in a way that separates noise from the actual content, the network differentiates between genuine features in the image and noise patterns caused by Gaussian blur. The DnCNN's data-driven approach allows it to learn intricate noise patterns, which involves filtering and smoothing the output of the CNN to refine the denoised image further. By eliminating the noise from the image, DnCNN effectively reduces blurring caused by noise-related artifacts.

4. Experimental Results and Analysis

4.1. Dataset

We used the IQ-OTHNCCD Lung Cancer Dataset, collected for three months in the fall of 2019, to evaluate our image denoising hybrid model. It was presented by Alyasriy et al. [55] and can be downloaded from: https://www.kaggle.com/code/adityamahimkar/lung-cancer-prediction-on-image-data, accessed on 17 December 2022. We used 1294 grayscale images of the IQ-OTHNCCD dataset, classified into normal, benign, and malignant. Each image was resized to 512 pixels wide × 512 pixels high for training and validation of our model. A total of 1035 images were used for training, and 259 images were used for testing. Among these images, 1096 were found to be affected by Gaussian blur noise, while 198 contained salt and pepper noise. In this work, the focus was primarily to address the dominant noise type, Gaussian blur noise.

A systematic approach was adopted to comprehensively assess the denoising performance and account for potential variations. The Gaussian blur noise was added to the images at different levels, ranging from 5% to 60% noise intensity levels. This range of noise intensity allowed for testing the denoising method's effectiveness under various noise levels. The addition of noise symmetrically from 5% through to 60% serves several purposes, including assessing the error margin even when noise levels deviate from the baseline and realism in real-world image conditions where noise levels vary. This approach ensures noise levels are tested against noise levels that represent a broad spectrum at optimal noise levels. The Gaussian blur noise was added by setting the standard deviation of the Gaussian noise distribution to 0.15. For training purposes, each image was converted into patch sizes of 45 × 45, resulting in 2200 patches per image.

The choice of dataset was made considering clinical realism and relevance reflecting typical CT image characteristics encountered in a real-world setting. The fact that the dataset was collected from various specialist hospitals over three months in the fall of 2019 relates to the current challenges faced by CT images. Furthermore, the dataset includes CT scans of patients diagnosed with lung cancer in different stages and healthy subjects, providing a real-world view.

4.2. Hyperparameters

Each instance of our image denoising approach requires an average of 0.0166667 s of computational time to complete the training phase. This duration reflects the computational resources invested in training a single model. Longer training times offer the potential for refined weight optimization and improved model performance, albeit at a higher resource cost. The proposed model used a learning rate of 0.00238. The learning rate governs the step size taken by the optimization algorithm during parameter updates. This updated value aims to strike a balance between convergence speed and stability. A higher learning rate can expedite convergence, but a careful balance is necessary to prevent overshooting and instability during optimization. We trained the model for a fixed 47 epochs. An epoch denotes a complete iteration through our training dataset. The number of epochs directly affects the frequency of weight updates using the complete dataset. An optimal number of epochs is crucial to mitigate underfitting and overfitting risks. Finally, we employed 846 steps per epoch to ensure comprehensive model training. A step involves updating the model parameters based on a data batch. This parameter, coupled with the batch size, determines the frequency of parameter updates. Higher steps enhance convergence, but computational requirements increase accordingly.

4.3. Qualitative Analysis

The qualitative analysis visually compared the denoised image with an original noisy image. Noise reduction and preservation of image details were observed, whereby the denoised image appeared smoother and cleaner than the noisy image, with reduced visual artifacts caused by noise. Additionally, the denoised image exhibited a similar structure and pattern as the original image, indicating effective denoising. The intensity profiles were

analyzed to assess the preservation of fine details. Intensity profiles are one-dimensional plots of pixel intensity values along a specific line or region of interest in the image. By comparing the intensity profiles of the denoised image with the original image, it verified whether important features and edges were well preserved in the denoised result. The qualitative analysis for denoising CT images is demonstrated in Figure 2.

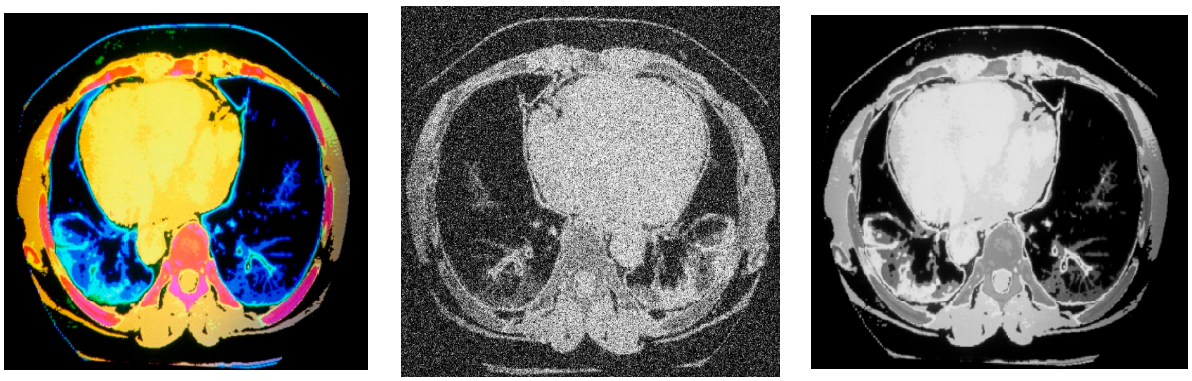

(**a**) Original Image (**b**) Noisy Image (30%) (**c**) Denoised Image

Figure 2. (**a**) Original image [55], (**b**) noisy image (30%), and (**c**) denoised image.

In Figure 2, the original image in (a) was applied with a grayscale filter in combination with an AGBN with a 30% noise level. The image was degraded after adding Gaussian blur noise, as shown in (b). The denoised image in (c) was generated by applying an anisotropic Gaussian filter, which suppressed the Gaussian noise while preserving edges by using more smoothing in the regions with little variations and less smoothing in the areas with solid intensity gradients. Anisotropic Gaussian filters enhanced the sharpness and overall image structure. Haar transform was then applied to decompose the noisy CT scan images into different frequency bands, including approximation and detail coefficients. Mainly, it analyzed and detected abrupt changes in intensity, such as edges in an image. Removing noise and lower-frequency components while retaining high-frequency information related to the edge helps enhance edge details and reduce blurring. Finally, the DnCNN was trained on a noisy and corresponding clean images dataset to learn the noise patterns and underlying structures. It took a noisy image as input during inference and used its learned knowledge to estimate and remove the noise. By eliminating the noise from the image, the DnCNN effectively reduced blurring caused by noise-related artifacts.

In Figure 3, the CT scan image was corrupted by adding a 5–30% Gaussian blur noise level. The addition of noise was necessary to obtain the measure of error margins when noise levels deviated. The focus was on reducing the AGBN, which had 1096 images, translating to 85% noisy images contaminated with AGBN. Figure 3 shows the original greyscale CT scan image and the denoised image using the proposed approach. Images R1 to R6 had Gaussian blur noise added at different noise intensities to allow for testing the denoising method's effectiveness under various noise levels, as shown in Figure 3.

The noisy images were denoised using wiener, mean, median, DWT, Gaussian, non-local means (NLM) filter, and DnCNN for selected CT scan images at various additive Gaussian blur noise (GBN) intensities (5–30% noise intensity) as shown in Figure 3a–f. As more noise is added to the image, blurring and visual quality increases. Image denoising techniques aim to improve the visual quality and interpretability of images by reducing the impact of noise which can otherwise degrade image quality and hinder the ability to extract meaningful information from the image. It was demonstrated that the proposed approach of wavelet–anisotropic Gaussian filter-based denoising CNN remarkably reduced the additive GBN, and at the same time, minimized the blurring effect and improved visual quality, achieving better image and fine details' preservation compared to other schemes used in the experiment.

Greyscale original image

Denoised image using proposed approach

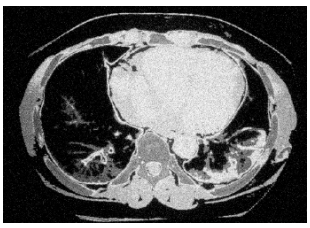

(**a**) Noisy image R1 at 5% AGBN intensity

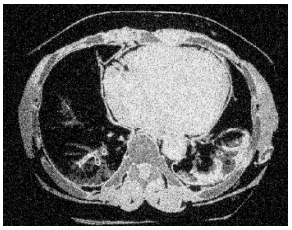

(**b**) Noisy image R2 at 10% AGBN intensity

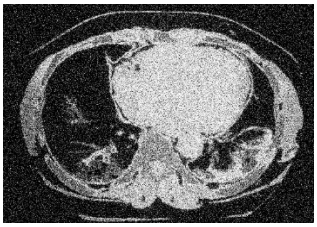

(**c**) Noisy image R3 at 15% AGBN intensity

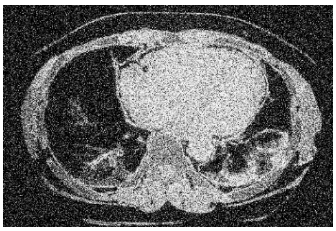

(**d**) Noisy image R4 at 20% AGBN intensity

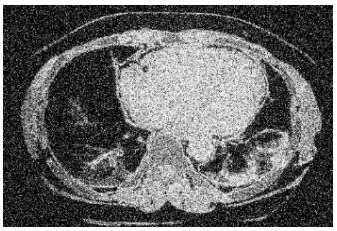

(**e**) Noisy image R5 at 25% AGBN intensity

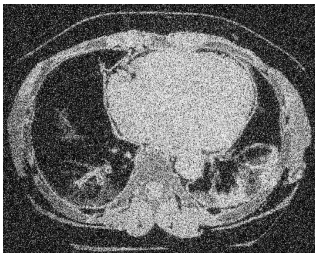

(**f**) Noisy image R6 at 30% AGBN intensity

Figure 3. CT scan images with added Gaussian blur noise at 5% to 30% noise intensities in figure (**a**–**f**).

4.4. Quantitative Analysis

The proposed approach was verified using a subjective analysis approach. The performance evaluators, such as peak signal-to-noise ratio (PSNR), structural similarity index measure (SSIM), signal-to-noise ratio (SNR), and mean squared error (MSE), were considered to quantify the result. The proposed wavelet-based image deblurring and restoration approach was evaluated together with other state-of-the-art denoising techniques using PSNR, SSIM, and MSE as representative quantitative measurements, as shown below.

PSNR is the ratio between the maximum possible power of a signal and the power of corrupting noise. The PSNR measures the peak signal-to-noise ratio between two images, used as the quality measurement between two images. The higher the value of PSNR, the better the quality of the compact image. PSNR is usually expressed in terms of the logarithmic decibel scale.

PSNR is calculated as:

$$\mathrm{PSNR}_{\mathrm{dB}} = 10\log_{10}\left(\frac{MAX^2}{MSE}\right) \tag{8}$$

$$= 20\log_{10}(MAX) - 10\log_{10}(MSE)$$

where:

MAX = maximum possible pixel value of the image,

MSE = mean square error.

The mean square error (*MSE*) is the cumulative error between the compressed and original images. The lower the *MSE*, the better the quality of the impermeable image. It is calculated as:

$$MSE = \frac{1}{pq}\sum_{a=0}^{p-1}\sum_{b=0}^{q-1}[I(a,b) - K(a,b)]^2 \quad (9)$$

where p q: dimensions of the image,

$I(a, b)$: intensity of pixels (a, b) in the original image,

$K(a, b)$: intensity of pixels (a, b) in denoised images.

The SSIM yields an objective assessment of the quality of the images. The SSIM depends on luminance, contrast, and structural terms. The product of these parameters is the SSIM of the image. The parameter $L(x_1, x_2)$ is the luminance assessment function that determines the quality of having only a tiny margin between two images in terms of mean luminance (μx_1 and μx_2).

The parameter $C(x_1, x_2)$ is the contrast assessment function that computes the quality of having only a tiny margin between two images in terms of standard deviations (σ_{x1} and σ_{x2}). The parameter $S(x_1, x_2)$ is the structure assessment function determining the correlation coefficient between two images regarding covariance (σ_{x1x2}).

$$\mathrm{SSIM}(x_1, x_2) = \lfloor L(x_1, x_2)\rfloor a_1 \times \lfloor C(x_1, x_2)\rfloor b_1 \times \lfloor S(x_1, x_2)\rfloor c_1 \quad (10)$$

where:

$$L(x_1, x_2) = \frac{2\mu_{x_1}\mu_{x_2} + U_1}{\mu_{x_1}^2 + \mu_{x_2}^2 + U_1}$$

$$C(x_1, x_2) = \frac{2\sigma_{x_1}\sigma_{x_2} + U_2}{\sigma_{x_1}^2 + \sigma_{x_2}^2 + U_2}$$

$$S(x_1, x_2) = \frac{\sigma_{x_1x_2} + U_3}{\sigma_{x_1}\sigma_{x_2} + U_3}$$

where μx_1 and μx_2 are the local means, σx_1 and σx_2 are the standard deviations, and (σ_{x1x2}) is the image's cross-covariance of x_1, x_2. Assume $a_1 = b_1 = c_1 = 1$, $U_1 = (R \times S_1)^2$ and $U_2 = (R \times S_2)^2$, where R is the size of the image (256 for 8-bit grayscale images), U_1 is a small constant value at $S_1 << 1$, U_2 is the positive constant value at $S_2 << 1$, and $U_3 = U_2/^2$.

The simplified version of SSIM is as follows:

$$\mathrm{SSIM}(x_1, x_2) = \frac{(2\mu_{x_1}\mu_{x_2} + U_1)(2\sigma_{x_1x_2} + U_2)}{(\mu_{x_1}^2 + \mu_{x_2}^2 + U_1)(\sigma_{x_1}^2 + \sigma_{x_2}^2 + U_2)} \quad (11)$$

4.5. Quantitative Results

The efficiency and performance of the proposed approach were validated and quantified by comparing the greyscale CT images with other well-known standard denoising filters, such as mean, median, Gaussian, wiener, non-local means (NLMs), and discrete wavelet transform (DWT) for additive Gaussian blur noise (AGBN) reduction using PSNR, SSIM, and MSE. The CT images R1, R2, R3, R4, R5, and R6 were used to compare the proposed approach with the standard filters for 5% to 60% noise intensity. Tables 1–5 in this section shows comparison of the proposed ensemble approach with other standard techniques and their performance in terms of PSNR, SNR and SSIM at various additive GBN noise intensities. Similarly Figures 4–9 reflect the performance of standard techniques and proposed ensemble approach for denoising additive Gaussian blur noise (AGBN).

Table 1. (a) PSNR comparison for the proposed approach with wiener, mean, median, DWT, Gaussian, non-local means (NLM) filter, and DnCNN for selected CT scan images at various additive Gaussian blur noise (GBN) intensities (5–30% noise intensity). (b) PSNR comparison for the proposed approach with wiener, mean, median, Gaussian, DWT, NLM filter, and DnCNN for selected CT scan images at various AGBN intensities (35–60% noise intensity).

PSNR						
Denoising Scheme	**Gaussian Blur Noise at Different Intensities (%)**					
	5%	**10%**	**15%**	**20%**	**25%**	**30%**
Non-Local Means [23]	29.6242	27.8872	26.1304	23.0332	19.9996	24.2514
Gaussian [24]	29.6897	28.7325	24.8656	21.7141	18.6318	22.9032
Median [25]	31.8468	28.9768	27.1306	22.0174	18.9910	13.2377
DWT [27]	30.9422	29.7876	27.1765	23.1353	19.9853	23.2240
Mean [28]	27.9920	27.9896	27.1805	19.0253	18.9953	21.6240
Wiener [42]	30.7984	27.8902	26.1477	20.9636	17.9785	22.1923
DnCNN [56]	31.9468	30.7896	28.5469	24.8696	20.9874	25.6457
Proposed Approach	34.7585	31.6760	29.2267	25.9174	21.4910	27.6377
PSNR						
Denoising Scheme	**Gaussian Blur Noise at Different Intensities (%)**					
	35%	**40%**	**45%**	**50%**	**55%**	**60%**
Non-Local Means [23]	22.0180	17.2751	18.3521	17.6835	17.1384	16.8923
Gaussian [24]	19.6064	15.6782	16.7898	16.2560	14.6484	15.1261
Median [25]	20.9886	16.0105	17.2122	16.5345	15.7932	15.5779
DWT [27]	23.1256	18.4231	18.4621	18.1563	17.5347	17.3223
Mean [28]	20.9682	16.0453	17.2301	16.5658	15.8584	15.3735
Wiener [42]	20.3963	15.0143	16.1786	15.4320	14.9675	14.8439
DnCNN [56]	25.9546	22.7896	22.6458	20.8976	20.9874	19.4865
Proposed Approach	27.0435	25.8896	24.9789	23.9453	22.5734	21.9547

Table 2. (a) SNR for different denoising schemes at various SPN noise intensities (5–30% noise intensity). (b) SNR for different denoising schemes at various SPN noise intensities (35% to 60%).

SNR Values						
Denoising Scheme	**Gaussian Blur Noise at Different Intensities (%)**					
	5%	**10%**	**15%**	**20%**	**25%**	**30%**
Non-Local Means [23]	22.7497	19.8691	18.0366	12.8525	9.8674	8.0812
Gaussian [24]	24.7053	23.7319	20.8656	14.7141	11.6318	9.9032
Median [25]	25.8455	21.9760	20.1306	15.0174	11.8910	10.2377
DWT [27]	22.4563	19.6455	17.8646	12.6789	9.4673	7.8956
Mean [28]	26.9982	22.9896	20.1805	18.0253	13.9653	10.2240
Wiener [42]	24.8508	21.8702	19.1477	15.9636	10.9785	9.1923
DnCNN [56]	20.0456	17.8654	16.9213	11.0486	7.9564	6.2893
Proposed Approach	18.6893	15.4563	15.0895	9.7987	6.8956	5.1124

Table 2. *Cont.*

Denoising Scheme	SNR Values					
	Gaussian Blur Noise at Different Intensities (%)					
	35%	40%	45%	50%	55%	60%
Non-Local Means [23]	6.8752	6.9932	5.0735	4.4100	3.8214	3.3328
Gaussian [24]	9.6175	7.6793	6.7695	6.2262	5.6484	5.1261
Median [25]	9.6986	8.1305	7.2202	6.5345	5.9930	5.4779
DWT [27]	6.5986	6.5467	5.0032	4.1264	3.4574	3.0042
Mean [28]	9.9898	8.1453	7.2461	6.5730	5.9483	5.4735
Wiener [42]	7.8863	7.0043	6.1846	5.4212	4.9325	4.4439
DnCNN [56]	5.6845	5.8697	4.7589	3.6895	2.8964	2.6874
Proposed Approach	4.6978	4.5535	2.8975	2.4967	2.1895	1.4984

Table 3. Comparison of MSE values of different filtering schemes, including wiener, mean, median, DWT, Gaussian, NLM filter, and DnCNN with the proposed approach for selected CT images R1, R2, R3, R4, R5, and R6.

IMAGE	Median [25]	Mean [28]	Wiener [42]	Gaussian [24]	NLM [23]	DWT [27]	DnCNN [56]	Proposed Approach
Image R1	29.7189	29.7290	24.5629	24.5736	39.3783	29.3783	29.2486	26.4634
Image R2	69.3731	69.9344	227.4001	218.8388	97.0323	85.0321	80.9547	70.9867
Image R3	236.6997	487.1047	575.0933	815.4983	137.1280	127.1280	111.8759	101.3453
Image R4	276.3539	526.7589	614.7475	855.1525	166.7822	156.7822	158.0136	135.6523
Image R5	325.3523	630.4532	640.8953	916.2461	186.0234	176.0234	165.8954	156.8953
Image R6	386.2341	689.2313	705.7646	947.9875	255.2488	245.3478	230.8694	206.9078

Table 4. SSIM values for images R1, R2, R3, R4, R5, and R6 at various noise intensities.

Noise Density	Image R1	Image R2	Image R3	Image R4	Image R5	Image R6
	SSIM Values					
5%	0.945185	0.943385	0.942513	0.937519	0.936408	0.934789
10%	0.926260	0.925201	0.924620	0.920162	0.919456	0.917345
15%	0.910734	0.910573	0.910914	0.905187	0.904893	0.904291
20%	0.901130	0.900996	0.898911	0.893868	0.893466	0.892968
25%	0.883405	0.883405	0.880901	0.876379	0.875789	0.874897
30%	0.865680	0.865809	0.863623	0.859061	0.858735	0.857798
35%	0.847955	0.847882	0.845612	0.840414	0.846746	0.846345
40%	0.830230	0.830382	0.828658	0.825006	0.825534	0.824784
45%	0.812505	0.812528	0.811728	0.810150	0.811231	0.810543

Table 5. Comparison of SSIM values of images R1, R2, R3, R4, R5, and R6 using the proposed approach and standard filtering schemes (wiener, mean, median, DWT, Gaussian, NLM, and DnCNN).

	SSIM Values							
CT Images	**Median [25]**	**Mean [28]**	**Wiener [42]**	**Gaussian [24]**	**NLM [23]**	**DWT [27]**	**DnCNN [56]**	**Proposed Approach**
Image R1	0.9796	0.9775	0.9863	0.9774	0.9834	0.9952	0.9987	1.000
Image R2	0.9570	0.9647	0.9589	0.9408	0.9694	0.9876	0.9899	1.000
Image R3	0.9418	0.9291	0.9335	0.9071	0.9712	0.9854	0.9887	1.0000
Image R4	0.9051	0.8934	0.9045	0.8703	0.9391	0.9591	0.9786	0.9967
Image R5	0.9042	0.8963	0.9123	0.9278	0.9545	0.9589	0.9785	0.9796
Image R6	0.8964	0.9121	0.9345	0.9221	0.9486	0.9675	0.9897	0.9986

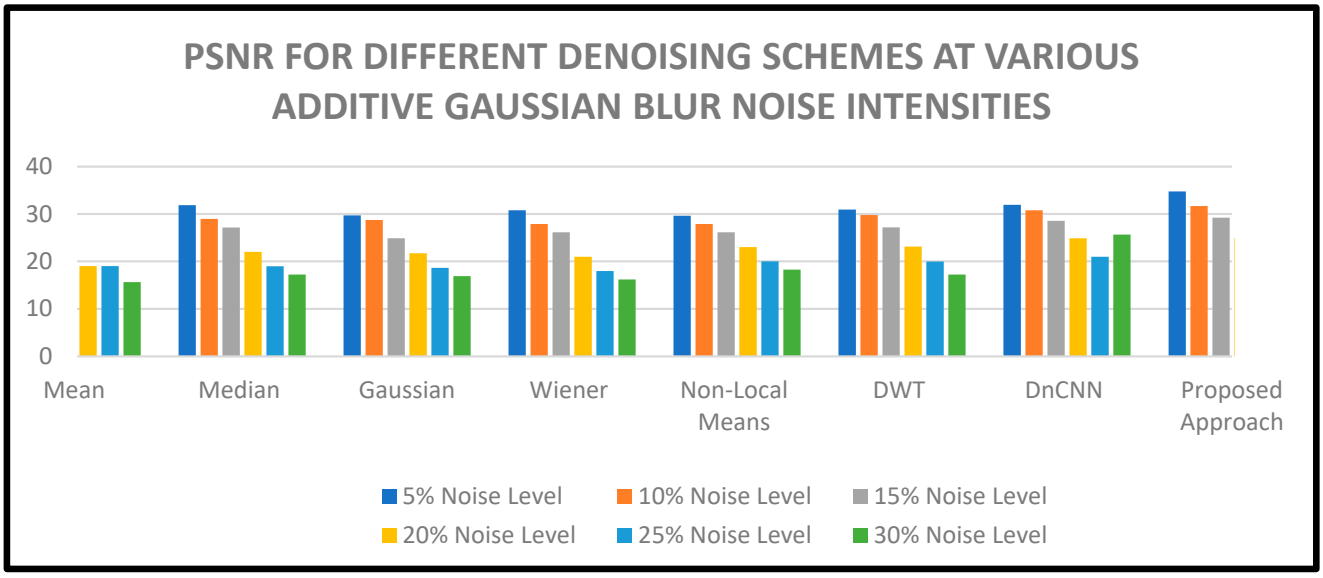

(**a**)

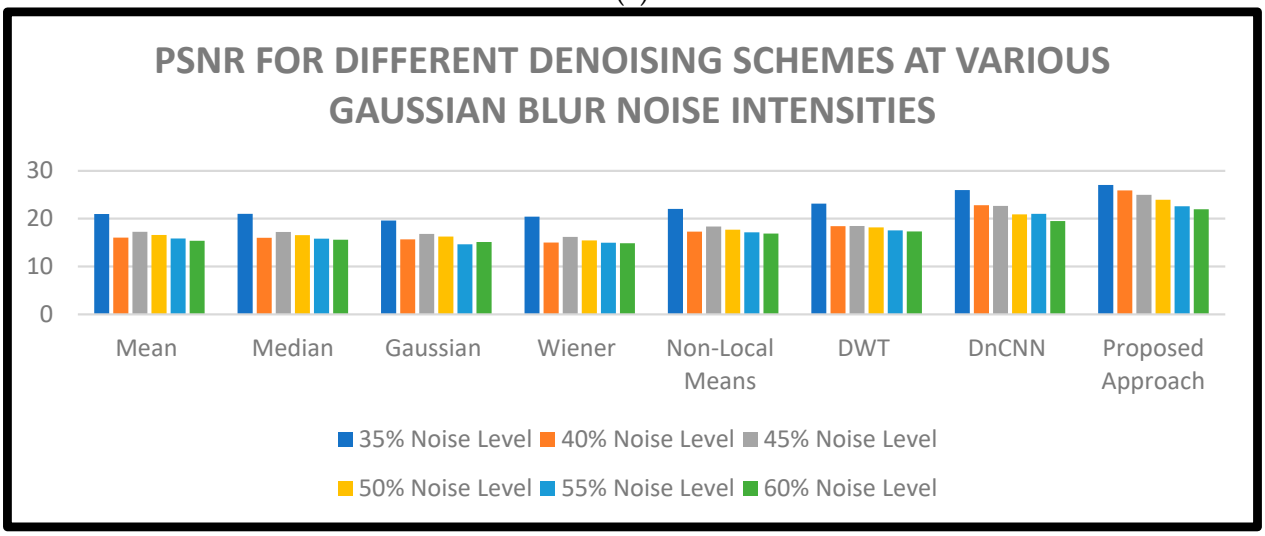

(**b**)

Figure 4. (**a**) PSNR for different denoising schemes at various AGBN intensities for images R1, R2, R3, R4, R5, and R6 (5–30% noise intensity). (**b**) PSNR for different denoising schemes at various AGBN intensities for images R1, R2, R3, R4, R5, and R6 (35–60% noise intensity).

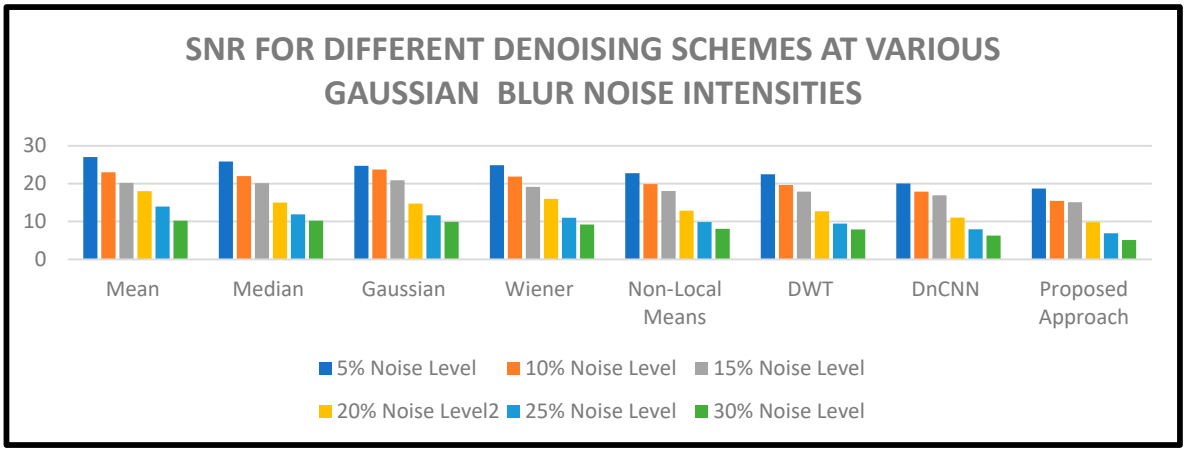

(**a**)

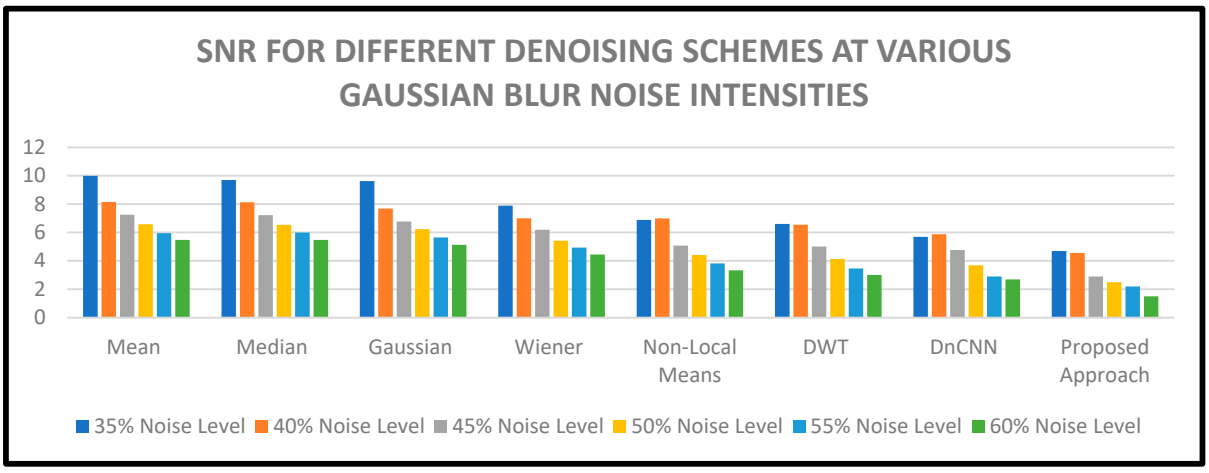

(**b**)

Figure 5. (**a**) SNR for different denoising schemes at various SPN noise intensities (5–30% noise intensity. (**b**) SNR for different denoising schemes at various SPN noise intensities (35% to 60%).

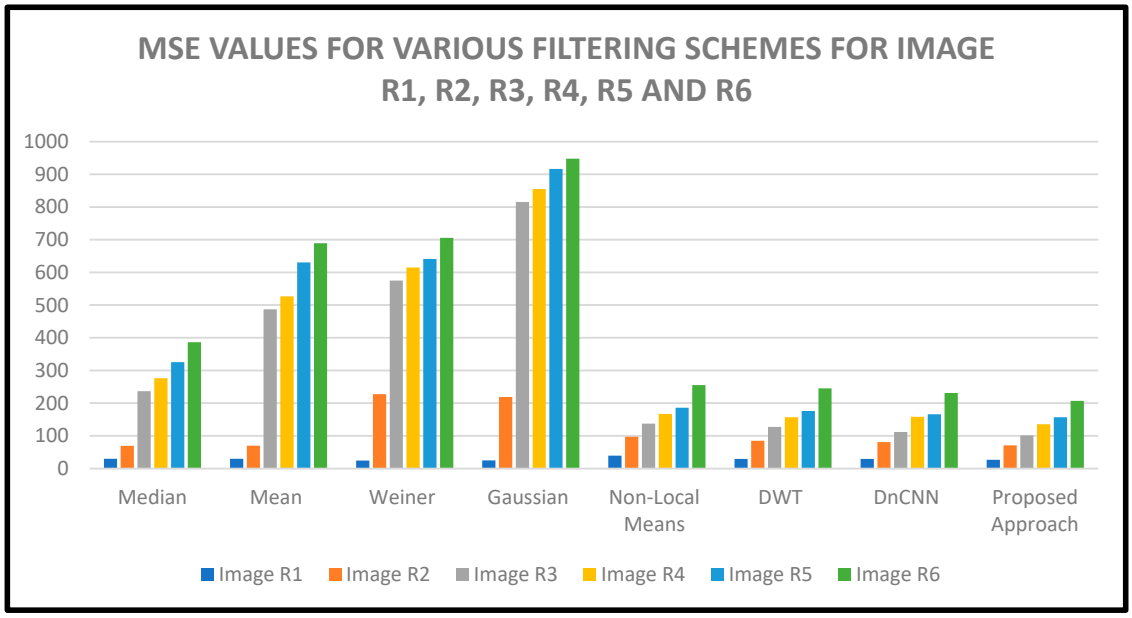

Figure 6. Graph comparison of MSE values of different filtering schemes and the proposed approach for CT images R1, R2, R3, R4, R5, and R6.

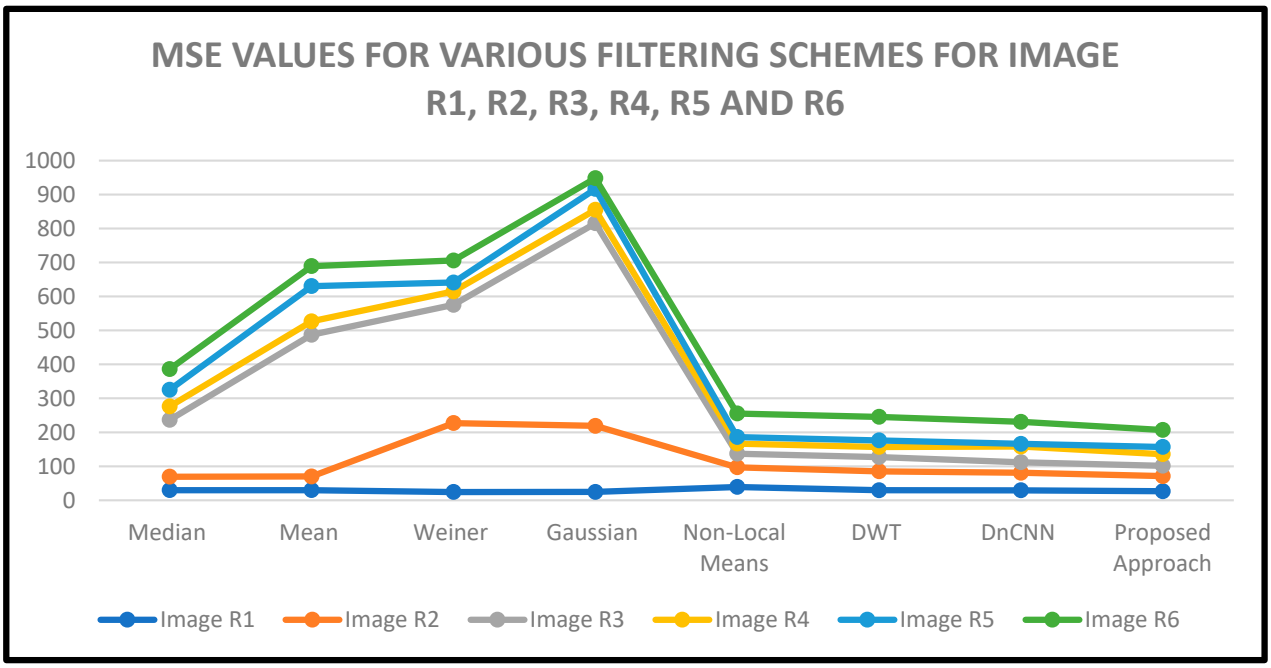

Figure 7. Linear comparisons of MSE values of different filtering schemes and the proposed approach for CT images R1, R2, R3, R4, R5, and R6.

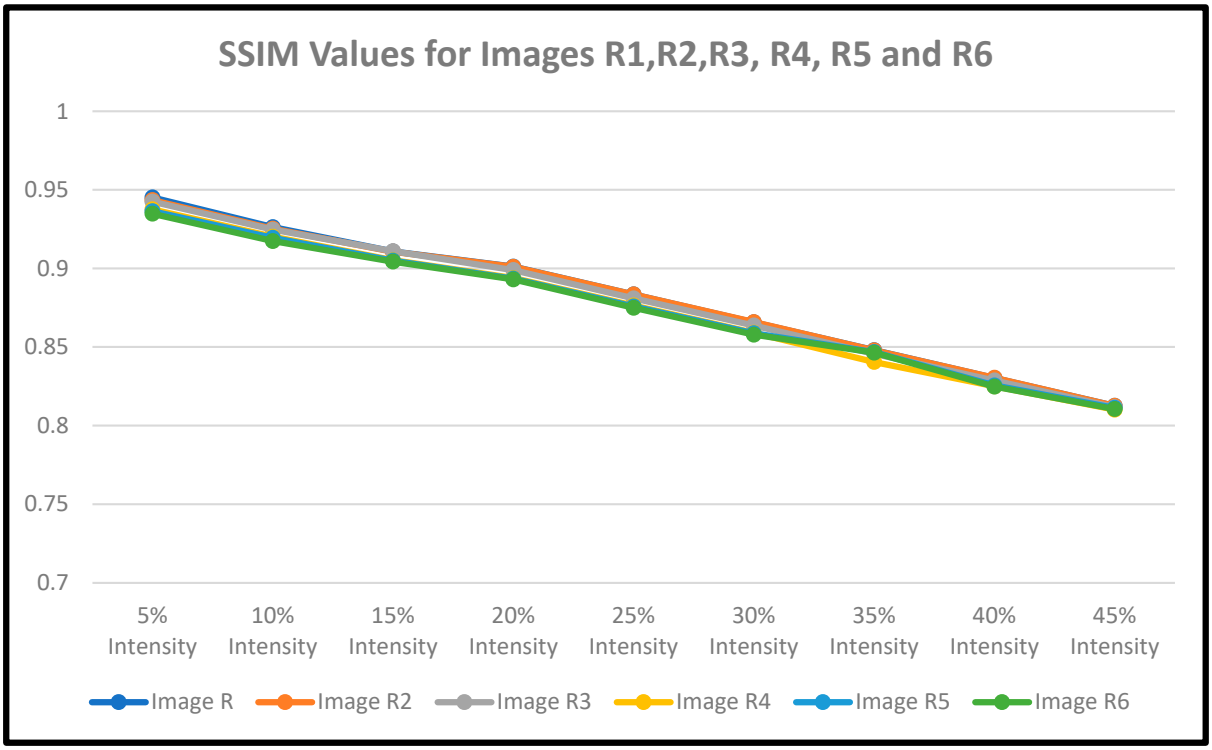

Figure 8. Linear graph depicting SSIM values for CT images R1, R2, R3, R4, R5, and R6 at various AGBN intensities.

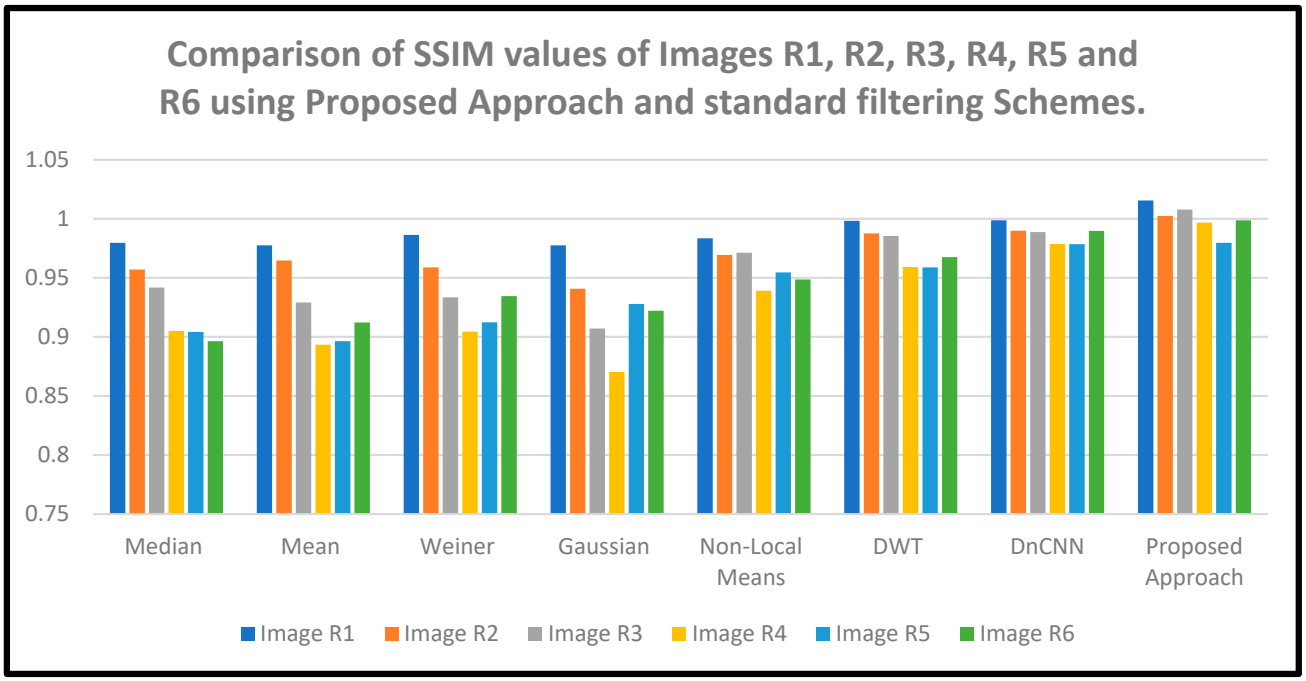

Figure 9. Graph for the comparison of SSIM values of images R1, R2, R3, R4, R5, and R6 using the proposed approach and standard filtering schemes.

5. Discussion

The performance of the proposed ensemble approach was evaluated using the PSNR, SSIM, and MSE metrics. PSNR quantifies the denoised image quality relative to the original noisy image. It measures the ratio between the maximum signal power of the original image and the noise power affecting the denoised image. A higher PSNR score signifies greater image fidelity. The SSIM values ranging between 0 and 1 mean that 1 ideally matches the reconstructed image with the original image. The ensemble approach effectively denoised within a computational time of 0.01666 s, optimizing the trade-off between model performance and resource consumption. The updated learning rate of 0.00238 struck an improved balance between convergence speed and optimization stability, enhancing the overall training efficiency. The training for 47 epochs ensured comprehensive weight optimization and reduced the risks of underfitting or overfitting. Using 846 steps per epoch and a batch size of 45 $\times$ 45 facilitated faster convergence while managing the computational demands. The PSNR metric validated the high quality of our denoised images, as evidenced by elevated PSNR scores indicating substantial image fidelity. The proposed approach performed better than previous experiments in [24,56], whereby our proposed approach achieved PSNR values of 34.7585, 31.6760, 29.2267, 21.4910, and 27.6377, respectively.

6. Conclusions

Computed tomography (CT) is a commonly used imaging modality that provides diagnostic information for medical images. In this study, 1294 CT medical images were used, whereby 1096 were affected by Gaussian blur noise, while 198 were affected by salt and pepper noise. Gaussian blur noise (GBN) in the images degrades the visual quality and restoration of the image. This research primarily focused on Gaussian blur noise, which dominated 85% of the images. To thoroughly evaluate the denoising capabilities and accommodate possible fluctuations, a systematic methodology was implemented. Gaussian blur noise was added to the images at varying levels, ranging from 5% to 60% in noise intensity. This diverse spectrum of noise intensities facilitated the assessment of the denoising techniques' efficacy across a range of noise levels. This study proposed a

wavelet-based anisotropic Gaussian filter (AGF) and denoising CNN to remove noise in CT scan medical images. The Haar wavelet transform and AGF were used as preprocessing operations. The process started by adding Gaussian blur noise to the medical images, and the generated noisy images were then denoised using AGF. Haar transform further decomposed the denoised CT scan image into different frequency bands.

The DnCNN was combined with AGF and wavelet Haar transform for post-processing. This study employed six CT scan images: R1, R2, R3, R4, R5, and R6 (grayscale images), for experimental analysis. The standard denoising filters, such as median, mean, wiener, Gaussian, NLM, DWT, and DnCNN, were applied to denoise the images affected by additive Gaussian blur noise, whose performance was compared with the proposed approach, whereby measurements were performed in Python, and the PSNR, SSIM, and MSE values were measured. The results from Table 1 and Figure 4, revealed that the proposed ensemble approach yielded the best results for PSNR at different additive Gaussian blur noise intensities from 5% to 60%. In Table 1, the PSNR values for the proposed approach were higher than other standard denoising filter schemes at 34.7585, 31.6760, 29.2267, 24.9174, 21.4910, and 27.6377 in a range of 5% to 30% noise intensities, respectively. This was closely followed by DnCNN results at 31.9468, 30.7896, 28.5469, 20.9874, and 25.6457, respectively. When the PSNR was high, the MSE between the original and reconstructed images was very low. Therefore, this implies that the image was adequately restored, and the restored image quality was finer.

The resultant SSIM index is a decimal value between -1 and 1, where 1 indicates perfect similarity, 0 indicates no similarity, and -1 indicates perfect anti-correlation.

Consequently, if the PSNR value is low, the quality of the restored image could be better. The proposed approach aims to reduce all types of Gaussian noise, and the central feature is that the noise-free pixels are left unchanged. The proposed approach performed better than previous experiments, demonstrating its efficiency and suitability for denoising CT scan medical images. The SSIM index is a decimal value that range between -1 and 1. A value of 1 indicates that the two images are very similar or the same, while a value of 0 demonstrates that the two images are very different and no similarity and -1 indicates perfect anti-correlation. These values are often adjusted to the range of [0, 1], where the extremes hold the same meaning. The SSIM values in Table 5 for the proposed approach were 1.000, 1.000, 1.0000, 0.9967, 0.9796, and 0.9986, respectively. Since the SSIM values range between 0 and 1, 1 perfectly matches the reconstructed image with the original image. It is observed that the proposed approach had higher SSIM values in comparison to other denoising methods used in this study. The values were at or near 1.0, implying a more exceptional structural similarity between the denoised and original CT images. It was observed that, in all the scenarios considered, increasing the density of Gaussian blur noise led to decreasing the SSIM values; however, even increasing the noise density, where noise density $d \in \{5\%, 10\%, 15\%, 20\%, 25\%, 30\%, 35\%, 40\%, 45\%, 50\%, 55\%, 60\%\}$, the SSIM values for the proposed approach were still higher in comparison to other techniques tested. When comparing the general performance of the proposed approach to other standard filtering techniques and CNN-based methods, it was observed that our approach outperformed the others when applied to the IQ-OTHNCCD dataset. The results highlight the denoising technique's effectiveness and efficiency for CT scan images.

Author Contributions: Conceptualization, T.K.A.; methodology, T.K.A. and R.M.R.; experimentation, T.K.A., R.M.R., and G.O.O.; original draft preparation, T.K.A. and R.M.R.; review and editing, T.K.A. and G.O.O.; funding acquisition, T.K.A. and G.O.O. All authors have read and agreed to the published version of the manuscript.

Funding: This research received no external funding.

Institutional Review Board Statement: Not applicable.

Informed Consent Statement: Not applicable.

Data Availability Statement: Data are contained within the article.

Conflicts of Interest: The authors declare no conflict of interest.

References

1. Alanazi, T.M.; Berriri, K.; Albekairi, M.; Ben Atitallah, A.; Sahbani, A.; Kaaniche, K. New Real-Time High-Density Impulsive Noise Removal Method Applied to Medical Images. *Diagnostics* **2023**, *13*, 1709. [CrossRef]
2. Tian, C.; Fei, L.; Zheng, W.; Xu, Y.; Zuo, W.; Lin, C.W. Deep learning on image denoising: An overview. *Neural Netw.* **2020**, *131*, 251–275. [CrossRef] [PubMed]
3. Kadhim, M.A. Restoration Medical Images from Speckle Noise Using Multifilters. In Proceedings of the 2021 7th International Conference on Advanced Computing and Communication Systems (ICACCS), Coimbatore, India, 19–20 March 2021; Volume 1, pp. 1958–1963.
4. Satra, H.; Gupta, A. Lung Nodule Detection using Segmentation Approach for Computed Tomography Scan Images. *Int. J. Forresearch Appl. Sci. Eng. Technol.* **2021**, *9*, 1778–1790. [CrossRef]
5. Das, K.P.; Chandra, J. A Review on Preprocessing Techniques for Noise Reduction in PET-CT Images for Lung Cancer. In *Congress on Intelligent Systems: Proceedings of CIS 2021*; Springer Nature: Singapore, 2022; Volume 2, pp. 455–475.
6. Choi, H.; Jeong, J. Despeckling algorithm for removing speckle noise from ultrasound images. *Symmetry* **2020**, *12*, 938. [CrossRef]
7. Bharati, S.; Khan, T.Z.; Podder, P.; Hung, N.Q. A comparative analysis of image denoising problem: Noise models, denoising filters and applications. In *Cognitive Internet of Medical Things for Smart Healthcare: Services and Applications*; Springer: Berlin/Heidelberg, Germany, 2021; pp. 49–66.
8. Rausch, I.; Mannheim, J.G.; Kupferschläger, J.; la Fougère, C.; Schmidt, F.P. Image quality assessment along the one-metre axial field-of-view of the total-body Biograph Vision Quadra PET/CT system for 18F-FDG. *Ejnmmi Phys.* **2022**, *9*, 87. [CrossRef]
9. Goyal, B.; Agrawal, S.; Sohi, B.S. Noise issues prevail in various types of medical images. *Biomed. J.* **2018**, *11*, 1227.
10. Florez-Aroni, S.M.; Hancco-Condori, M.A.; Torres-Cruz, F. Noise Reduction in Medical Images. *arXiv* **2023**, arXiv:2301.01437.
11. Bhonsle, D.; Bagga, J.; Mishra, S.; Sahu, C.; Sahu, V.; Mishra, A. Reduction of Gaussian noise from Computed Tomography Images using Optimized Bilateral Filter by Enhanced Grasshopper Algorithm. In Proceedings of the 2022 Second International Conference on Advances in Electrical, Computing, Communication and Sustainable Technologies (ICAECT), Bhilai, India, 21–22 April 2022; pp. 1–9.
12. Hermena, S.; Young, M. CT-scan image production procedures. In *StatPearls [Internet]*; StatPearls Publishing: Treasure Island, FL, USA, 2022.
13. Nakamura, Y.; Higaki, T.; Tatsugami, F.; Honda, Y.; Narita, K.; Akagi, M.; Awai, K. Possibility of deep learning in medical imaging focusing on improvement of computed tomography image quality. *J. Comput. Assist. Tomogr.* **2020**, *44*, 161–167. [CrossRef]
14. Kaur, A.; Dong, G. A Complete Review on Image Denoising Techniques for Medical Images. *Neural Process Lett.* **2023**, *55*, 7807–7850. [CrossRef]
15. Mehta, D.; Padalia, D.; Vora, K.; Mehendale, N. MRI image denoising using U-Net and Image Processing Techniques. In Proceedings of the 2022 5th International Conference on Advances in Science and Technology (ICAST), Mumbai, India, 2–3 December 2022; pp. 306–313.
16. Xu, J.; Gong, E.; Ouyang, J.; Pauly, J.; Zaharchuk, G. Ultra-low-dose 18F-FDG, brain PET/MR denoising, using deep learning and multi-contrast information. In *Medical Imaging 2020: Image Processing*; SPIE: Bellingham, WA, USA, 2020; Volume 11313, pp. 420–432.
17. Kim, B.; Han, M.; Shim, H.; Baek, J. Performance comparison of convolutional neural network-based image denoising methods: The effect of loss functions on low-dose CT images. *Med. Phys.* **2019**, *46*, 3906–3928. [CrossRef]
18. Sagheer, S.V.M.; George, S.N. A review on medical image denoising algorithms. *Biomed. Signal Process. Control* **2020**, *61*, 102036.
19. Kaur, J.; Goyal, B.; Dogra, A. An Analysis of Different Noise Removal Techniques in Medical Images. In *Advances in Signal Processing, Embedded Systems, and IoT: Proceedings of Seventh ICMEET-2022*; Springer Nature: Singapore, 2023; pp. 579–590.
20. Thakur, R.S.; Chatterjee, S.; Yadav, R.N.; Gupta, L. Medical image denoising using convolutional neural networks. In *Digital Image Enhancement and Reconstruction*; Academic Press: Cambridge, MA, USA, 2023; pp. 115–138.
21. Abdelhamed, A.; Timofte, R.; Brown, M.S. Ntire 2019 challenge on actual image denoising: Methods and results. In Proceedings of the IEEE/CVF Conference on Computer Vision and Pattern Recognition Workshops, Long Beach, CA, USA, 16–20 June 2019; pp. 1–14.
22. Vimala, C.; Aruna Priya, P.; Subramani, C. Wavelet transform approach for image processing–A research motivation for engineering graduates. *Int. J. Electr. Eng.* **2021**, *58*, 373–384. [CrossRef]
23. Zhang, X. A modified non-local means using bilateral thresholding for image denoising. *Multimed. Tools Appl.* **2023**, 1–22. [CrossRef]
24. Mayasari, R.; Heryana, N. Reduce Noise in Computed Tomography Images using Adaptive Gaussian Filter. *arXiv* **2019**, arXiv:1902.05985.
25. Ştefănigă, S.A. Fine-Tuned Medical Images Denoising using Median Filtering. *Appl. Med. Inform.* **2021**, *43*, 27.
26. Juneja, M.; Joshi, S.; Singla, N.; Ahuja, S.; Saini, S.K.; Thakur, N.; Jindal, P. Denoising of computed tomography using bilateral median-based autoencoder network. *Int. J. Imaging Syst. Technol.* **2022**, *32*, 935–955. [CrossRef]
27. Ismael, A.A.; Baykara, M. Digital Image Denoising Techniques Based on Multi-resolution Wavelet Domain with Spatial Filters: A Review. *Trait. Du Signal* **2021**, *38*, 639–651. [CrossRef]

28. Anam, C.; Adi, K.; Sutanto, H.; Arifin, Z.; Budi, W.S.; Fujibuchi, T.; Dougherty, G. Noise reduction in CT images using a selective mean filter. *J. Biomed. Physicsengineering* **2020**, *10*, 623. [CrossRef]
29. Diwakar, M.; Singh, P. CT image denoising using the multivariate model and its method of noise thresholding in the non-subsampled shearlet domain. *Biomed. Signal Process. Control* **2020**, *57*, 101754. [CrossRef]
30. Sumijan, S.S.; Purnama, A.W.; Arlis, S. Peningkatan Kualitas Citra CT-Scan dengan Penggabungan Metode Filter Gaussian dan Filter Median. *J. Teknol. Inf. Dan Ilmu Komput.* **2019**, *6*, 591–600. [CrossRef]
31. Chillaron, M.; Vidal, V.; Verdu, G. Evaluation of image filters for their integration with LSQR computerized tomography reconstruction method. *PLoS ONE* **2020**, *15*, e0229113. [CrossRef]
32. El-Shafai, W.; Mahmoud, A.; Ali, A.; El-Rabaie, E.; Taha, T.; Zahran, O.; El-Fishawy, A.S.; Soliman, N.F.; Alhussan, A.A.; Abd El-Samie, F. Deep cnn model for multimodal medical image denoising. *Comput. Mater. Contin* **2022**, *73*, 3795–3814. [CrossRef]
33. Yue, Z.; Zhao, Q.; Zhang, L.; Meng, D. Dual adversarial network: Toward real-world noise removal and noise generation. In Proceedings of the Computer Vision–ECCV 2020: 16th European Conference, Glasgow, UK, 23–28 August 2020; Part X 16. Springer International Publishing: Berlin/Heidelberg, Germany; pp. 41–58.
34. Xu, J.; Huang, Y.; Cheng, M.M.; Liu, L.; Zhu, F.; Xu, Z.; Shao, L. Noisy-as-clean: Learning self-supervised denoising from corrupted images. *IEEE Trans. Image Process.* **2020**, *29*, 9316–9329. [CrossRef] [PubMed]
35. Aslam, M.A.; Munir, M.A.; Cui, D. Noise removal from medical images using hybrid filters of technique. *J. Phys. Conf. Ser.* **2020**, *1518*, 012061. [CrossRef]
36. You, N.; Han, L.; Zhu, D.; Song, W. Research on image denoising in edge detection based on wavelet transform. *Appl. Sci.* **2023**, *13*, 1837. [CrossRef]
37. Liang, H.; Zhao, S. Salt and Pepper Noise Suppression for Medical Image by Using Non-local Homogenous Information. In *Cognitive Internet of Things: Frameworks, Tools and Applications*; Springer: Cham, Switzerland, 2020; pp. 189–199.
38. Garg, B. Restoration of highly salt-and-pepper-noise-corrupted images using a novel adaptive trimmed median filter. *Signal Image Video Process.* **2020**, *14*, 1555–1563. [CrossRef]
39. Gupta, S.; Sunkaria, R.K. Real-time salt and pepper noise removal from medical images using a modified weighted average filtering. In Proceedings of the 2017 the Fourth International Conference on Image Information Processing (ICIIP), Shimla, India, 21–23 December 2017; pp. 1–6.
40. Usui, K.; Ogawa, K.; Goto, M.; Sakano, Y.; Kyougoku, S.; Daida, H. Quantitative evaluation of deep convolutional neural network-based image denoising for low-dose computed tomography. *Vis. Comput. Ind. Biomed. Art* **2021**, *4*, 21. [CrossRef]
41. Kim, B.G.; Kang, S.H.; Park, C.R.; Jeong, H.W.; Lee, Y. Noise level and similarity analysis for computed tomographic thoracic image with fast non-local means denoising algorithm. *Appl. Sci.* **2020**, *10*, 7455. [CrossRef]
42. Sarita, D.R.; Saini, J. Assessment of De-noising Filters for Brain MRI T1-Weighted Contrast-Enhanced Images. In *Emergent Converging Technologies and Biomedical Systems: Select Proceedings of ETBS 2021*; Springer: Singapore, 2022; pp. 607–613.
43. Wang, J.; Tang, Y.; Zhang, J.; Yue, M.; Feng, X. Convolutional neural network-based image denoising for synchronous temperature measurement and deformation at elevated temperature. *Optik* **2021**, *241*, 166977. [CrossRef]
44. Goceri, E. Evaluation of denoising techniques to remove speckle and Gaussian noise from dermoscopy images. *Comput. Biol. Med.* **2022**, *152*, 106474. [CrossRef]
45. Majeeth, S.S.; Babu, C.N.K. Gaussian noise removal in an image using fast guided filter and its method noise thresholding in medical healthcare application. *J. Med. Syst.* **2019**, *43*, 1–9. [CrossRef] [PubMed]
46. Elhoseny, M.; Shankar, K. Optimal Bilateral Filter and convolutional neural network-based denoising method of medical image measurements. *Measurement* **2019**, *143*, 125–135. [CrossRef]
47. Ebrahimnejad, J.; Naghsh, A. Adaptive Removal of high-density salt-and-pepper Noise (ARSPN) for robust ROI detection used in watermarking brain MRI images. *Comput. Biol. Med.* **2021**, *137*, 104831. [CrossRef]
48. Li, C.; Li, J.; Luo, Z. An impulse noise removal model algorithm based on the logarithmic image before the medical image. *Signal Image Video Process.* **2021**, *15*, 1145–1152. [CrossRef]
49. Taufiq, U.A.; Anam, C.; Hidayanto, E.; Naufal, A. Automatic Placement of Regions of Interest using Distance transform to Measure Spatial Resolution on the Clinical Computed Tomography Images: A Pilot Study. *Int. J. Sci. Res. Sci. Technol.* **2022**, *9*, 462–471.
50. Arnal, J.; Súcar, L. Fast Method Based on Fuzzy Logic for Gaussian-Impulsive Noise Reduction in CT Medical Images. *Mathematics* **2022**, *10*, 3652. [CrossRef]
51. Suneetha, A.; Srinivasa Reddy, E. Robust Gaussian noise detection and removal in color images using modified fuzzy set filter. *J. Intell. Syst.* **2020**, *30*, 240–257. [CrossRef]
52. Li, R.; Zheng, B. A spatially adaptive hybrid total variation model for image restoration under Gaussian plus impulse Noise. *Appl. Math. Comput.* **2022**, *419*, 126862. [CrossRef]
53. Yuan, Q.; Peng, Z.; Chen, Z.; Guo, Y.; Yang, B.; Zeng, X. The edge-preserving median filter and weighted coding with sparse non-local regularization for the low-dose CT image denoising algorithm. *J. Healthc. Eng.* **2021**, *2021*, 6095676. [CrossRef]
54. Shah, V.H.; Dash, P.P. Two-stage self-adaptive cognitive neural network for mixed noise removal from medical images. *Multimed. Tools Appl.* **2023**, 1–23. [CrossRef]

55. Alyasriy, H.; Muayed, A.H. The IQ-OTHNCCD lung cancer dataset. *Mendeley Data* **2020**, *1*, 1–13. [CrossRef]
56. Wang, F.; Huang, H.; Liu, J. Variational-based mixed noise removal with CNN deep learning regularization. *IEEE Trans. Image Process.* **2019**, *29*, 1246–1258. [CrossRef] [PubMed]